International Journal of ChemTech Research
CODEN(USA): IJCRGG ISSN : 0974-4290
Vol.5, No.5, pp 2252-2266, July-Sept 2013

CFD Simulation Of Solid Concentration Distribution In A Flat Bottom Agitated Vessel Using Rushton Turbine

D.Chitra* and L.Muruganandam

Chemical Engineering Division, School of Mechanical and Building sciences,Vellore Institute of Technology University, Vellore-632014, India.

***Corres. Author: dchitra@vit.ac.in**
Phone:91-416-2202595

Abstract: Computational Fluid Dynamics (CFD) studies in a baffled stirred tank agitated by six bladed turbine rotating at 300 rpm is reported in this paper. This work is concerned with the effect of small range of particle size and particle density on solid concentration distribution in a baffled tank agitated vessel stirred with Rushton turbine. The system studied consisted of a cylindrical flat bottom tank, 294 mm in diameter, with six blades Rushton turbine, 98 mm in diameter, filled with water. Baffle width is 0.1 tank diameter and the impeller clearance is 0.3 tank diameter from the tank bottom. The height of liquid level in the tank is equal to tank diameter. The solid concentration was analyzed for different suspensions sand, granite, silica and quartz of different diameters 500 µm, 650 µm, 920 µm and 1100 µm using CFD tool CFX 12.0. A classical Eulerian-Eulerian two fluids model and the standard k- ε turbulence model were used to simulate the suspension behavior. In this work, the solid concentration distribution was predicted using frozen rotor steady state approach. It was observed that the solid concentration in the radial direction is similar for different particle sizes except near the wall and it was same for different density particles which is considered in this paper. Also the solid concentration in the axial direction had similar pattern for different density particles and different sizes. It is found that the solid volume fraction is decreases with increase in particle size and density at all heights in radial direction and it is more significant at higher suspension levels. The study revealed that non uniformity in solid concentration is viewed both in radial and axial direction at this speed for this close range of particle sizes and densities.
Keywords: Agitated vessel, solid suspension, solid concentration distribution, CFD simulation.

1.INTRODUCTION

Solid – liquid mixing is important in chemical engineering operations such as adsorption, crystallization, dissolution, leaching, ion exchange, precipitation and catalytic reactions.

Several studies on solid-liquid mixing system have been done for characterizing just suspended condition. Other parameters such as solid concentration distribution, cloud height, power consumption and scale up have not been studied extensively. Solid concentration distribution is one of the important features of solid-liquid stirred tank. Proper design of solid-liquid stirred tank requires sound knowledge of solid concentration profile in an agitated tank. Solid distribution in agitated vessels depends on different parameters, namely impeller type, impeller clearance, impeller speed, solid loading and physical properties of solid and liquid.

Many methods are available for predicting solid distribution in agitated tank. These include optical method[1,2], sample withdrawal method[3,4], iso-kinetic sampling[5,6], two electrode conductivity probe method[7], four electrode conductivity probe method[8], electrical resistance tomography method[9] and optical fiber

method[10]. Several authors have used phenomenological models such as one dimensional sedimentation dispersion model [11], multi zone sedimentation dispersion model [12], two or three dimensional network of zones model [13] to predict the solid concentration. CFD also have been used to predict the solid concentration distribution with different techniques [14, 15, 16, and 17].

An attempt has been made to study the effect of particle size and density on solid concentration distribution using Rushton turbine in a flat bottom agitated vessel. The model developed was validated with the experimental results from literature review, and then the model was used to simulate the solid concentration distribution. The present study uses a Computational Fluid Dynamics (CFD) package, CFX 12, to simulate the solid concentration distribution in an agitated tank.

2. CFD MODEL

2.1 Model equation

The simulation was carried out with the help of the commercial code ANSYS CFX 12.0. An Eulerian-Eulerian multi fluid model was used to describe the flow behavior primary and secondary phase. In this model, both liquid and solid were treated as interpenetrating continua represented by a volume fraction at each point of the system. The continuity and momentum equations are

$$\frac{\partial(\alpha_i\ \rho_i)}{\partial t} + \nabla.(\alpha_i\ \rho_i\overrightarrow{u_i}) = 0$$

Where α,ρ and u are volume fraction, density and velocity vector, respectively.

$$\frac{\partial\ (\alpha_i\ \rho_i\vec{u}_i\ )}{\partial t} + \nabla.(\alpha_i\ \rho_i\vec{u}_i\vec{u}_i) = -\alpha_i\nabla p_i + \nabla\cdot\left(\alpha_i\mu_i\left(\nabla\vec{u}_i + \left(\nabla\vec{u}_i\right)^T\right)\right) + \vec{F}_C + \vec{F}_i + \alpha_i\rho_i\vec{g}$$

Where p is pressure, μ is viscosity and g is gravity. F_C represents the centrifugal and Coriolis forces acting on phase i due to phase j.

2.2 Equations for turbulence

The standard k-ε model was used to describe the turbulent fluid flow. The relevant k and ε transport equations for the continuous phase are given below:

$$\frac{\partial}{\partial t}(\alpha_l\rho_l k_l) + \nabla\cdot(\alpha_l\rho_l\vec{u}_l k_l) = \nabla\cdot\left[\alpha_l\left(\mu_l + \frac{\mu_{tl}}{\sigma_k}\right)\nabla k_l\right] + \alpha_l P_l - \alpha_l\rho_l\varepsilon_l$$

$$\frac{\partial}{\partial t}(\rho_l\alpha_l\varepsilon_l) + \nabla\cdot(\alpha_l\rho_l\vec{u}_l\varepsilon_l) = \nabla\cdot\left[\alpha_l\left(\mu_l + \frac{\mu_{tl}}{\sigma_\varepsilon}\right)\nabla\varepsilon_l\right] + \alpha_l\frac{\varepsilon_l}{k_l}(C_{\varepsilon 1}p_l - C_{\varepsilon 2}\rho_l\varepsilon_l)$$

Where $C_{\varepsilon 1}$, $C_{\varepsilon 2}$ and σ_ε are parameters in the standard k-ε model.

Liquid phase turbulent viscosity is calculated using Sato enhanced turbulence model. Solid phase turbulence is modeled using a zero equation model.

2.3 Interphase drag force

The interphase force consists of drag force, virtual mass force, Basset force, lift force and turbulent dissipation force. The influence of lift force and virtual mass force on solid concentration profile is smaller and basset force in most cases is much smaller than the drag force. So the interphase force can be expressed as

$$\vec{F}_i = \vec{F}_i^D + \vec{F}_i^T$$

Where $\vec{F}_i^D$ and $\vec{F}_i^T$ are drag force and interfacial force due to turbulent dissipation respectively.

The drag force term is obtained by

$$\vec{F}_{ls}^{D} = \frac{3}{4}\frac{C_{D,ls}}{d_s}\rho_l \alpha_s |\vec{u}_s - \vec{u}_l|(\vec{u}_s - \vec{u}_l)$$

Where the drag coefficient C_D is obtained by Schiller Naumann drag model:

$$C_{D,ls} = max\left(\frac{24}{Re}(1 + 0.15\, Re^{0.687}), 0.44\right)$$

$$Re = \frac{\mu_l d_s |\vec{u}_s - \vec{u}_l|}{\mu_l}$$

The turbulent dispersion force is calculated by Lopez de Bertodano model:

$$\vec{F}_{ls}^{T} = C_{TD} C_D \frac{\nu_{tl}}{\sigma_{tl}}\left(\frac{\nabla \alpha_s}{\alpha_s} - \frac{\nabla \alpha_l}{\alpha_l}\right)$$

Where C_{TD} is momentum transfer coefficient for the interphase drag force, σ_{tl} is liquid turbulent Schmidt number, ν_{tl} is turbulent viscosity, α_s and α_t is the solid and liquid phase volume fractions respectively.

3.METHODOLOGY AND BOUNDARY CONDITIONS

3.1. Vessel geometry

The operating conditions and the geometry of the vessel were selected same as those used in the experimental work presented by J.M.Nouri and J.H.Whitelaw (1992) for validation of the simulation results. Fig.1 shows the stirred tank with Rushton impeller. The cylindrical, flat bottom agitated tank diameter T=294 mm, equal to the liquid height H, equipped with four vertical baffles of width w=T/10.Agitation was provided with six bladed Rushton turbine with a diameter D=98 mm located at T/3 from the bottom of the vessel. The parameters of the impeller are listed in Table 1. The liquid used was water at room temperature. The solid phase was sand, granite, silica and quartz. The physical properties of solid and liquid are given in Table 2.The impeller speed was selected as N=300 rpm.

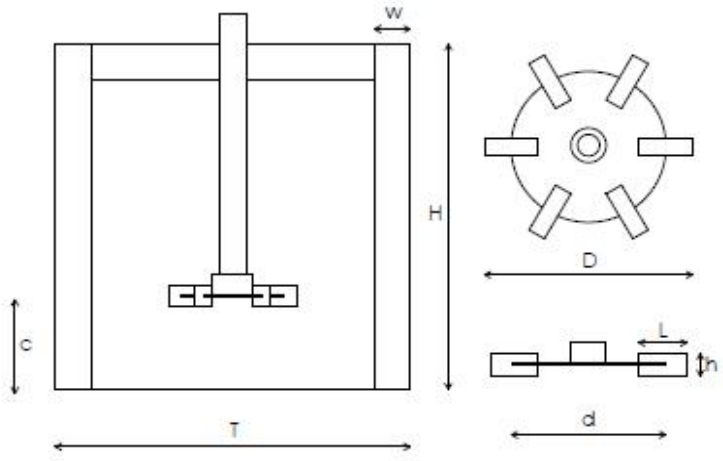

Fig. 1. Geometry of the agitation tank

Table 1.: Parameters of the impeller

	D	d	D_{hub}	L	h	t_{disc}
Value(m)	0.098	0.0735	0.0196	0.0245	0.0196	0.003

Table 2. : Physical properties of the solid-liquid system

	Liquid	Solid
Density (kg/m^3)	1000	2500(sand), 2550(Granite solid), 2600 (silica), 2650(Quartz),
Viscosity(Pa s)	$1x10^{-3}$	-
Particle diameter (µm)	-	500,650,920,1100
Volume fraction (vol%)	-	10

3.2. Numerical Simulation

The three dimensional steady state CFD model is employed to compute the solid concentration distribution in the stirred tank. Fig.2 shows half of the computational domain with baffles and stirrer. Due to rotational periodicity, half of the tank was simulated.

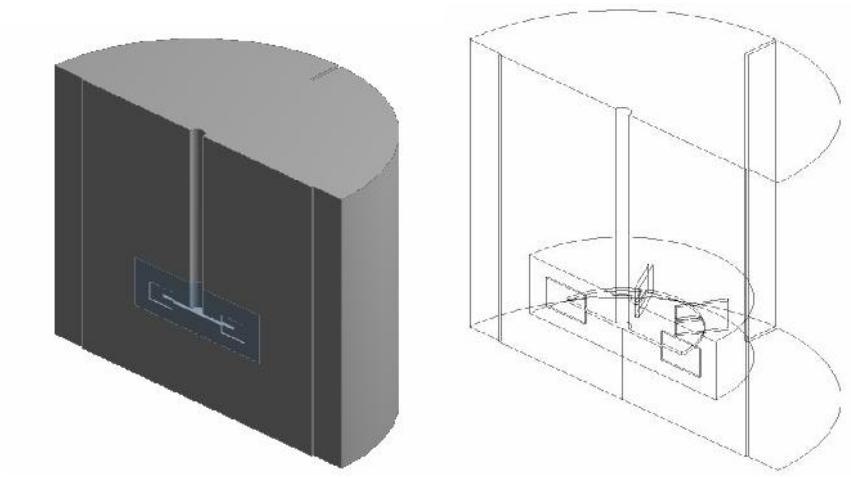

(a) **(b)**

Fig.2. Computational domain (a) solid (b) wireframe

The simulations of the stirred tank was performed by adopting Frozen rotor method coupled with multi fluid model and homogeneous two phase k-ε turbulence model in the commercial CFD code CFX -14. Frozen rotor analysis produces a steady state solution and this requires least amount of computational effort. The whole vessel was divided into two cylindrical domains as shown in Fig 3, one was an external domain containing the baffles and another was an inner domain containing the impeller. The computational domain was limited to π/2. The grid independency test was done by conducting simulations on total number of computational grid of 115460, 246440, and 350760 cells.

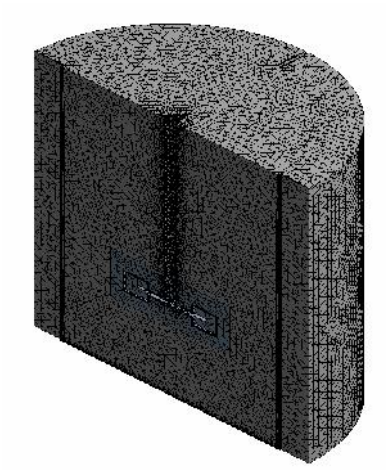

Fig.3. Computational grids.

The simulated results were compared with the experimental data, as shown in Fig.4. It shows a comparison of velocity profile between the simulated results and experimental results along the height for glass beads of diameter 232 µm, volumetric concentration 0.2% in water and speed of 300 rpm. Fig.5 shows a comparison of solid concentration distribution between the simulated results and experimental results along the height of the vessel at radius 20mm, diakon particle of diameter 665 µm, volumetric concentration 0.5% in mixture of tetraline and turpentine oil and speed of 313 rpm. It can be seen that the simulated results agree approximately with those determined experimentally. The grid of 246440 predicted a correct velocity profile and concentration distribution that did not change with further refinement of the grid. The simulation method was then expanded to study the solid concentration distribution inside the agitated tank.

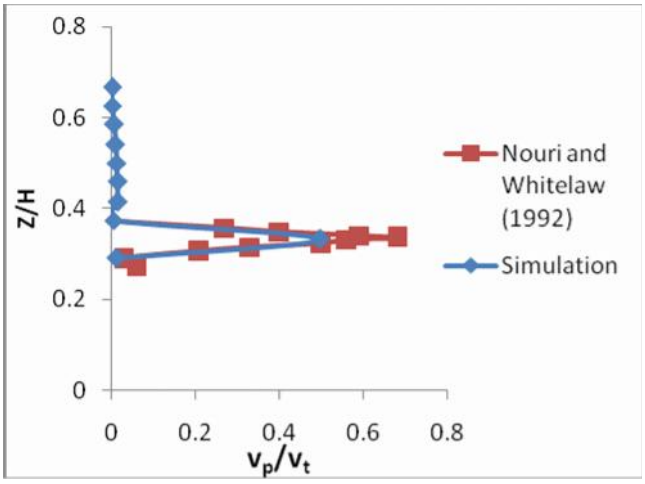

Fig. 4. Comparison of velocity profile between the simulated results and experimentalresults presented by J.M.Nouri and J.H.Whitelaw (1992)

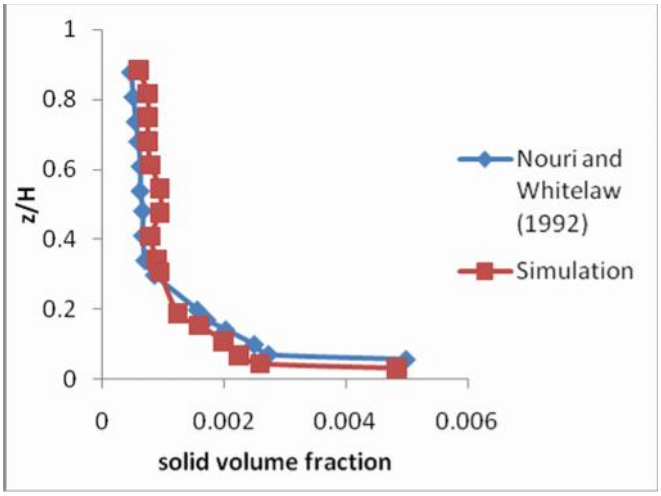

Fig. 5. Comparison of the solid concentration distribution between the simulated results and experimental results presented by J.M.Nouri and J.H.Whitelaw (1992)

4.RESULTS AND DISCUSSION

4.1 Volume fraction profiles

The simulated results of solids concentration maps for different condition both in radial and axial direction is shown in figs 5-7. The left figure shows vertical volume fraction distribution and right figure shows horizontal volume fraction distribution. Since the variation in particle size and density is closer the concentration maps looks similar.

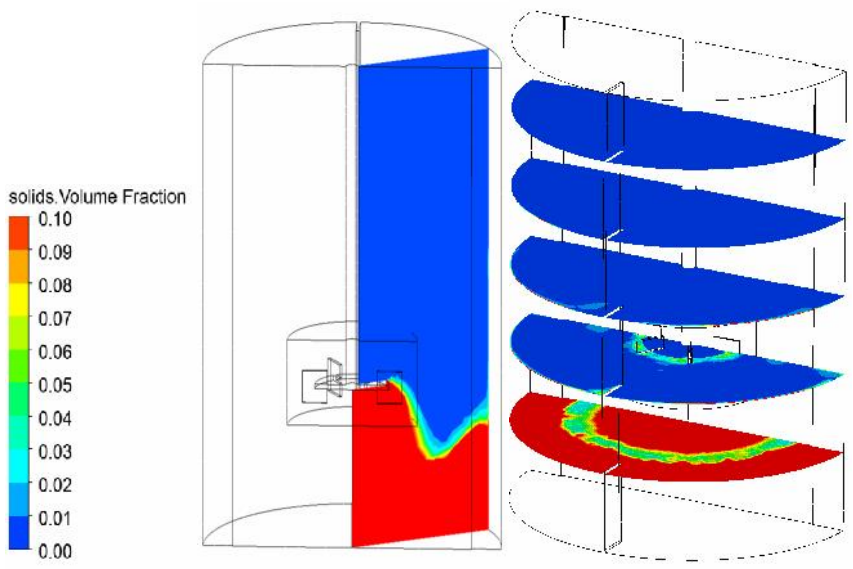

Fig.5. volume fraction of particle size 500 µm with density 2500 kg/m^3 and agitation speed of 300rpm.

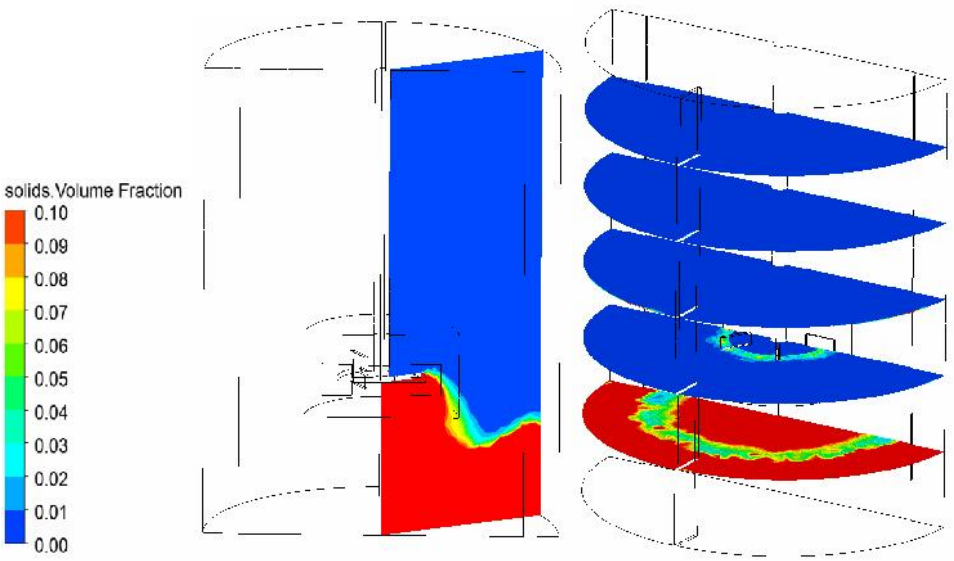

Fig. 6. Volume fraction of sand particle size 1100 µm with density 2500 kg/m^3 and agitation speed of 300rpm.

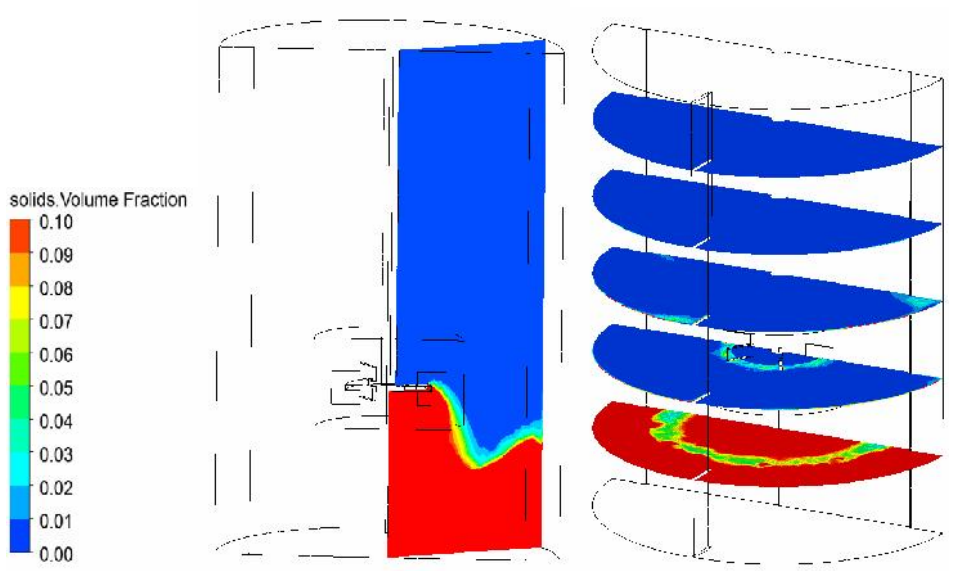

Fig. 7.Volume fraction of quartz (2650 kg/m^3) of size 1100 µm with agitation speed of 300rpm.

4.2 Radial concentration profile:

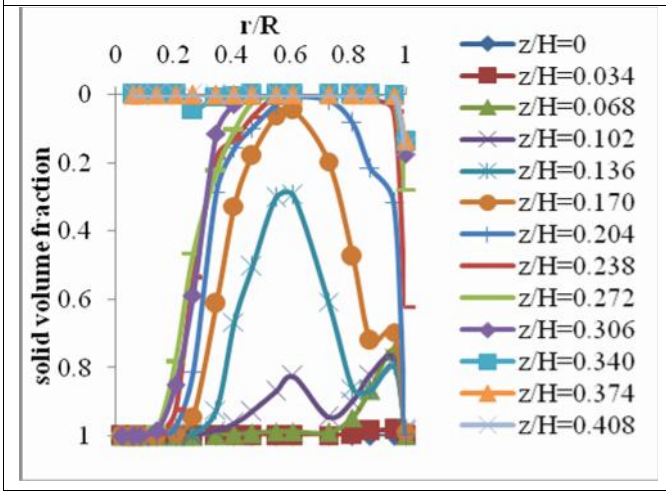

a

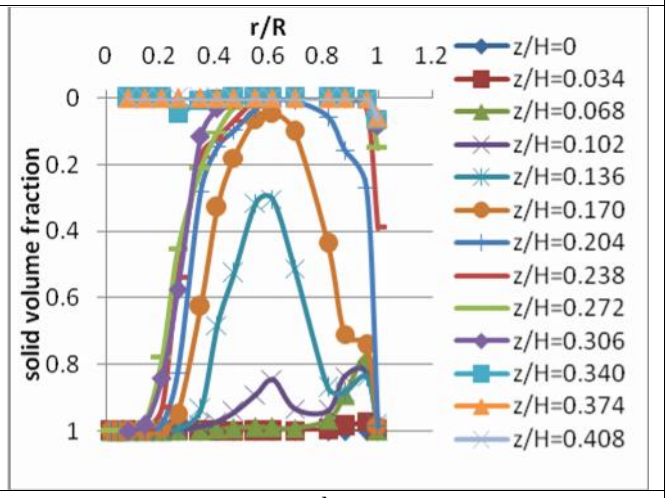

b

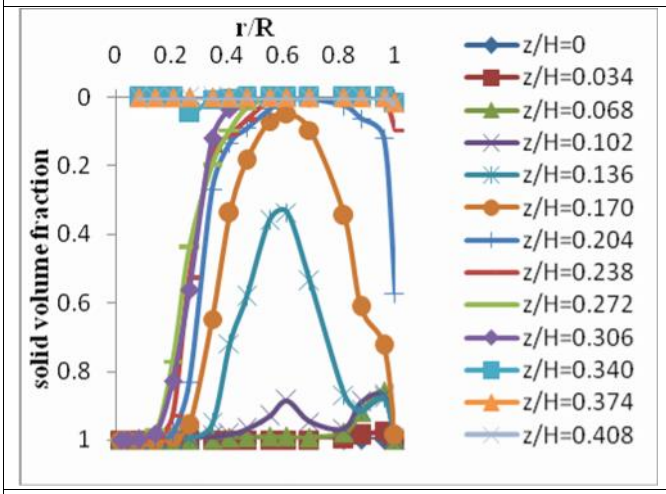

c

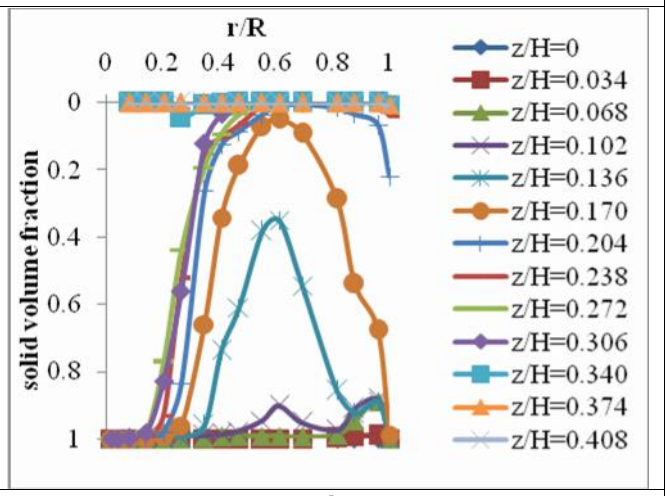

d

Fig. 8 The variation of solid volume fraction at various heights in radial direction for different particle sizes of sand (density 2500 kg/m^3) with a agitation speed of 300 rpm (a) 500 µm (b) 650 µm (c) 920 µm (d) 1100 µm

The variation of solid volume fraction at various heights for different particle sizes is shown in fig.8. The figure shows that the solid volume fraction profile is similar for all the particle sizes except near to the wall of the vessel. It can also be observed from the profile that the volume fraction closer to the wall decreases as the particle size increases, probably because of higher inertia of larger particles. Solid volume fraction is high at the bottom while it decreases dramatically along the vessel height.

It shows that volume fraction is uniform for all heights up to a radial distance of r/R=0.2. After this more variation is observed in solid volume fraction. It decreases up to a radial distance of r/R=0.6 and increases till r/R=0.9, after that steep increase in concentration is observed near the wall of the agitated vessel. The solid volume fraction have a minimum value and it is observed at r/R=0.6 and it is maximum near the wall for all heights and for all particle sizes. The cloud height for all particle sizes is observed at z/H=0.204. The similar graphs were also obtained for different solids of same size as given in fig.9.

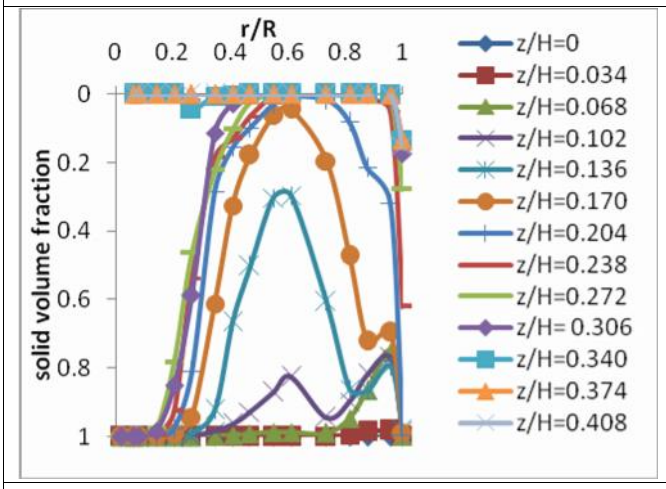

a

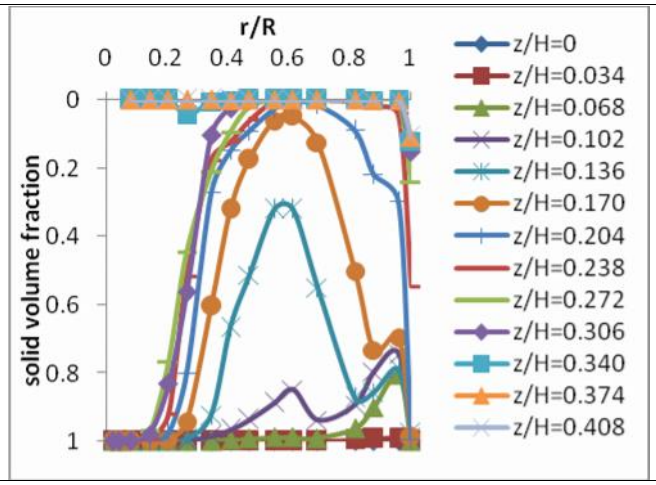

b

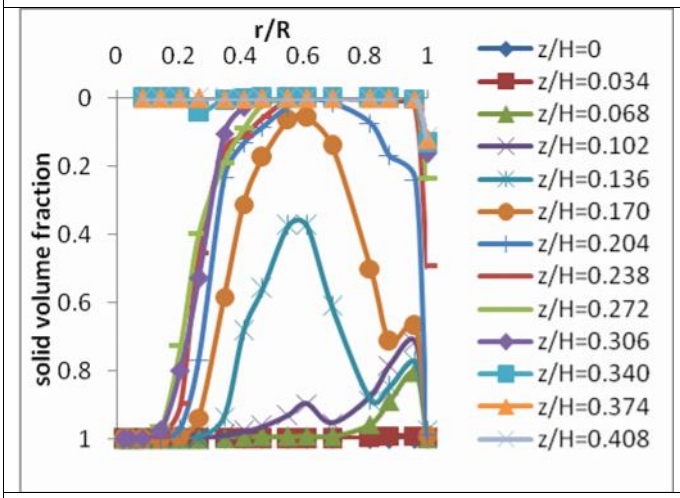

c

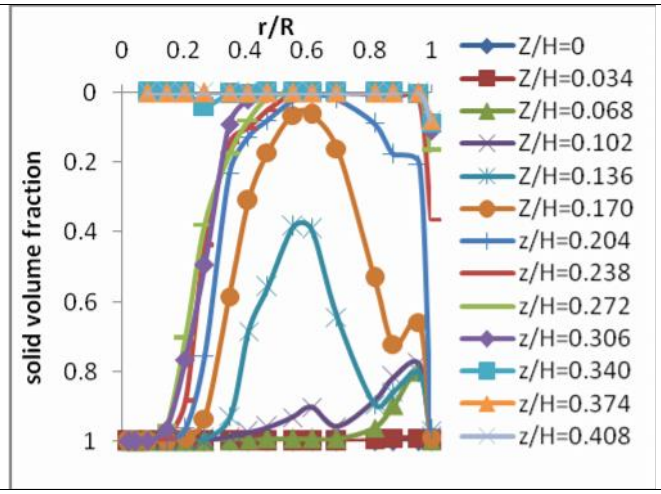

d

Fig 9. The variation of solid volume fraction at various heights in radial direction for different density solids with same diameter (a) Sand (2500 kg/m^3) (b) Granite solid (2550 kg/m^3) (c) Silica (2600 kg/m^3) (d) Quartz (2650 kg/m^3)

Axial concentration profile:

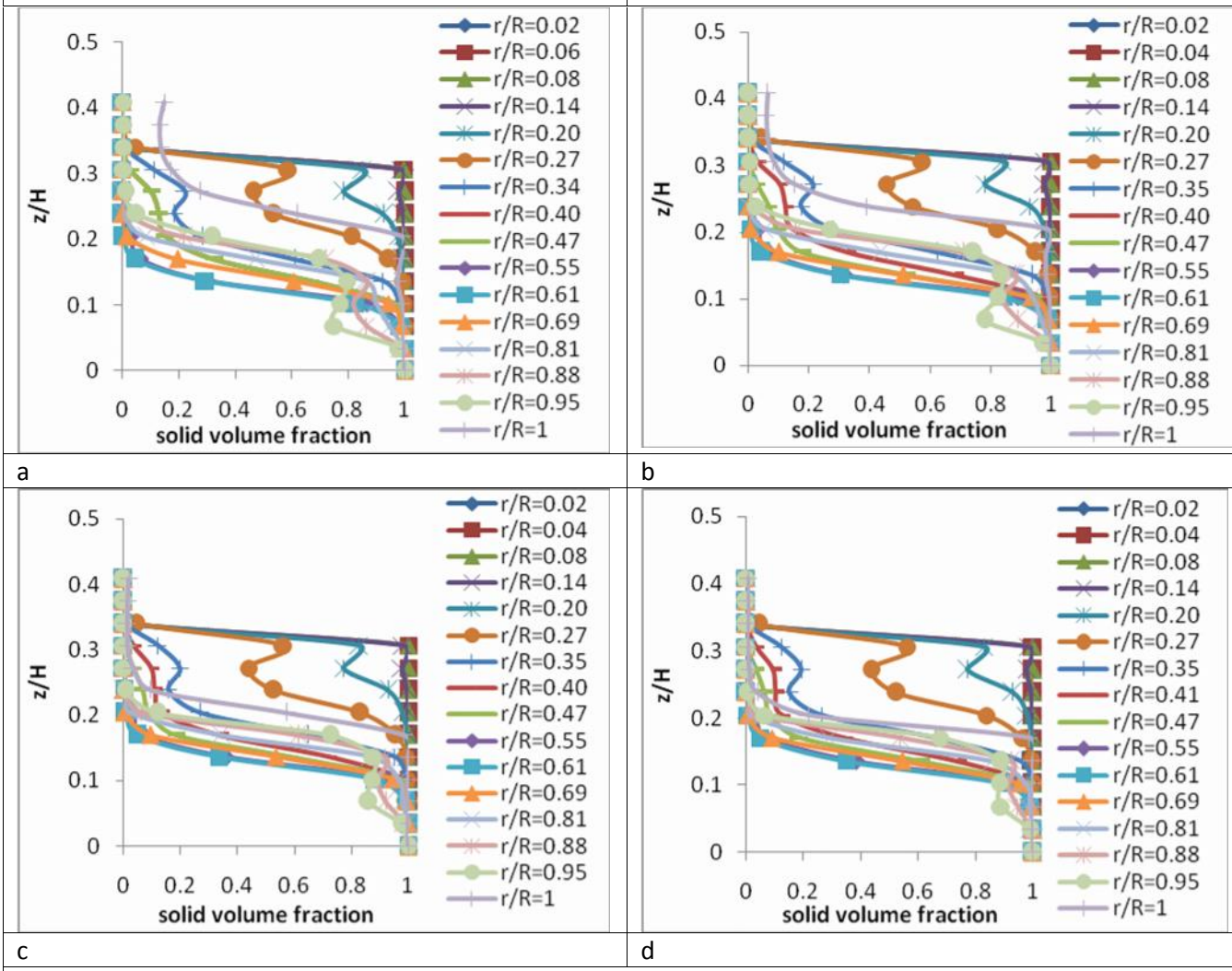

Fig.10 The variation of solid volume fraction at various radial position in axial direction for different particle sizes of sand (density 2500 kg/m^3) with a agitation speed of 300 rpm (a) 500 µm (b) 650 µm (c) 920 µm (d) 1100 µm

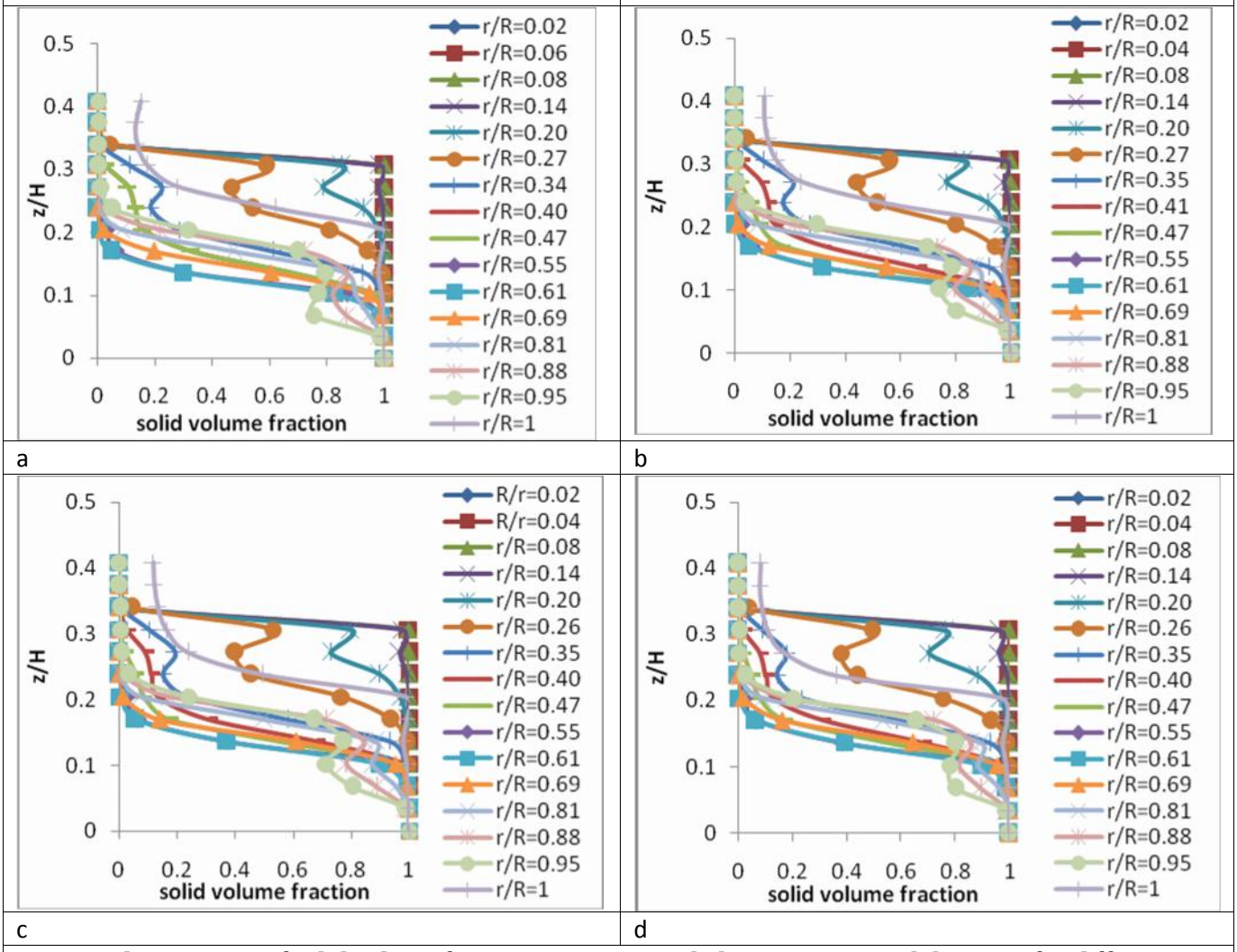

Fig. 11. The variation of solid volume fraction at various radial position in axial direction for different solids of same diameter 500 µm (a) Sand (2500 kg/m^3) (b) Granite solid (2550 kg/m^3) (c) Silica (2600 kg/m^3) (d)Quartz (2650 kg/m^3)

The simulated results of variation of solid volume fraction for different density solids at various heights and radial positions are shown in figure 10 and figure 11. The figure shows similar solid volume fraction profile both in radial and axial direction for different solids and it is non uniform. The solid concentration is high at the vessel bottom and it decreases dramatically along the vessel height. It was also observed that the profile flattens and continues to flatten as the radius increases. It shows that the axial homogeneity decreases towards the vessel wall.

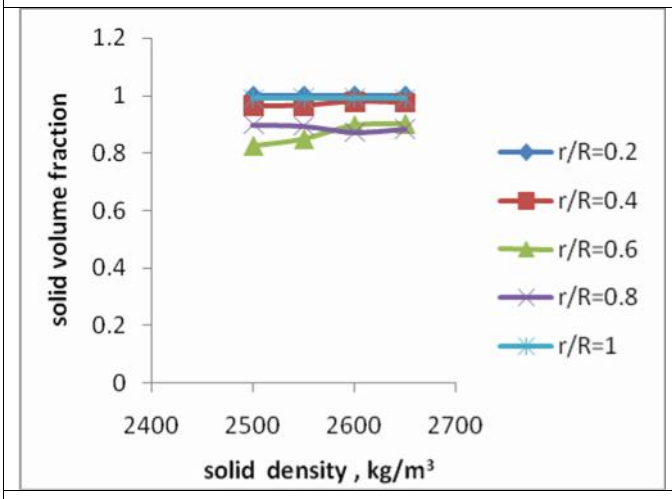

a

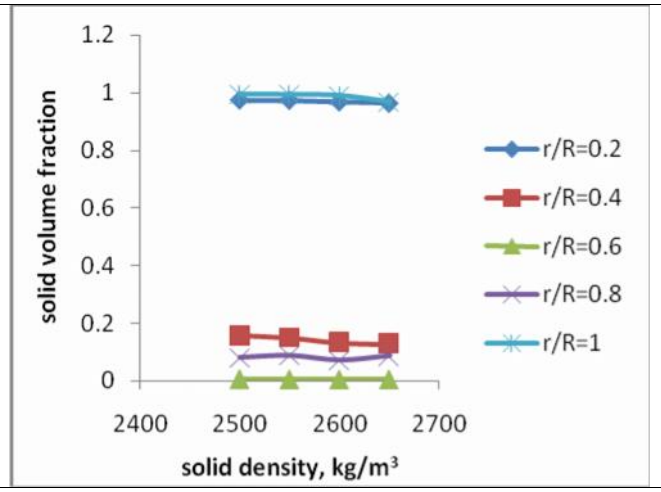

b

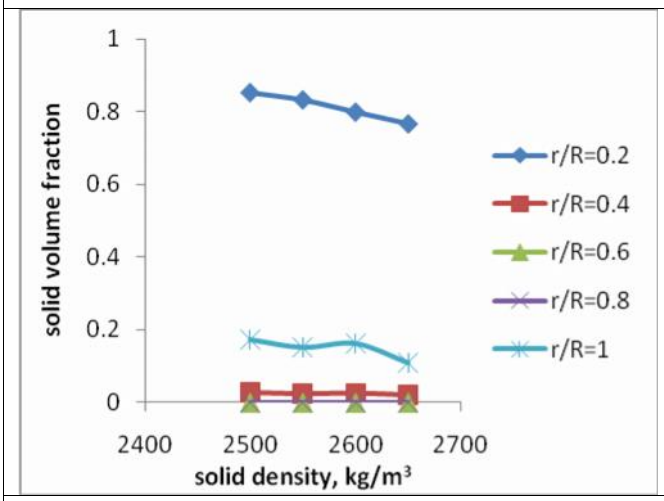

c

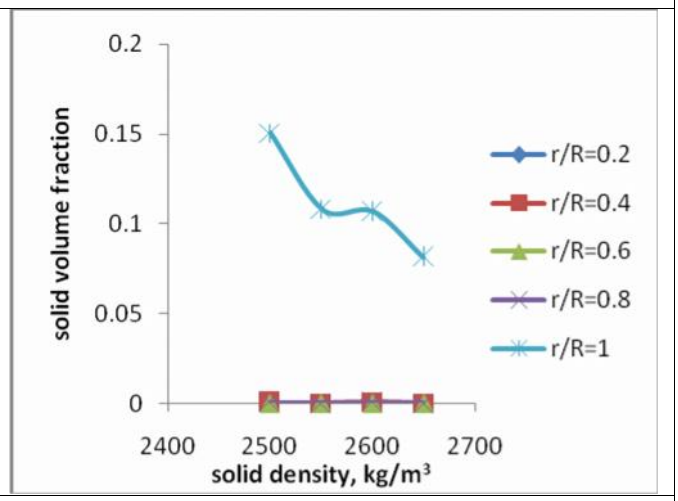

d

Fig .12. The variation of solid volume fraction for different solids at various heights (a) z/H=0.1 (b) z/H=0.2 (c) z/H=0.3 (d) z/H=0.4

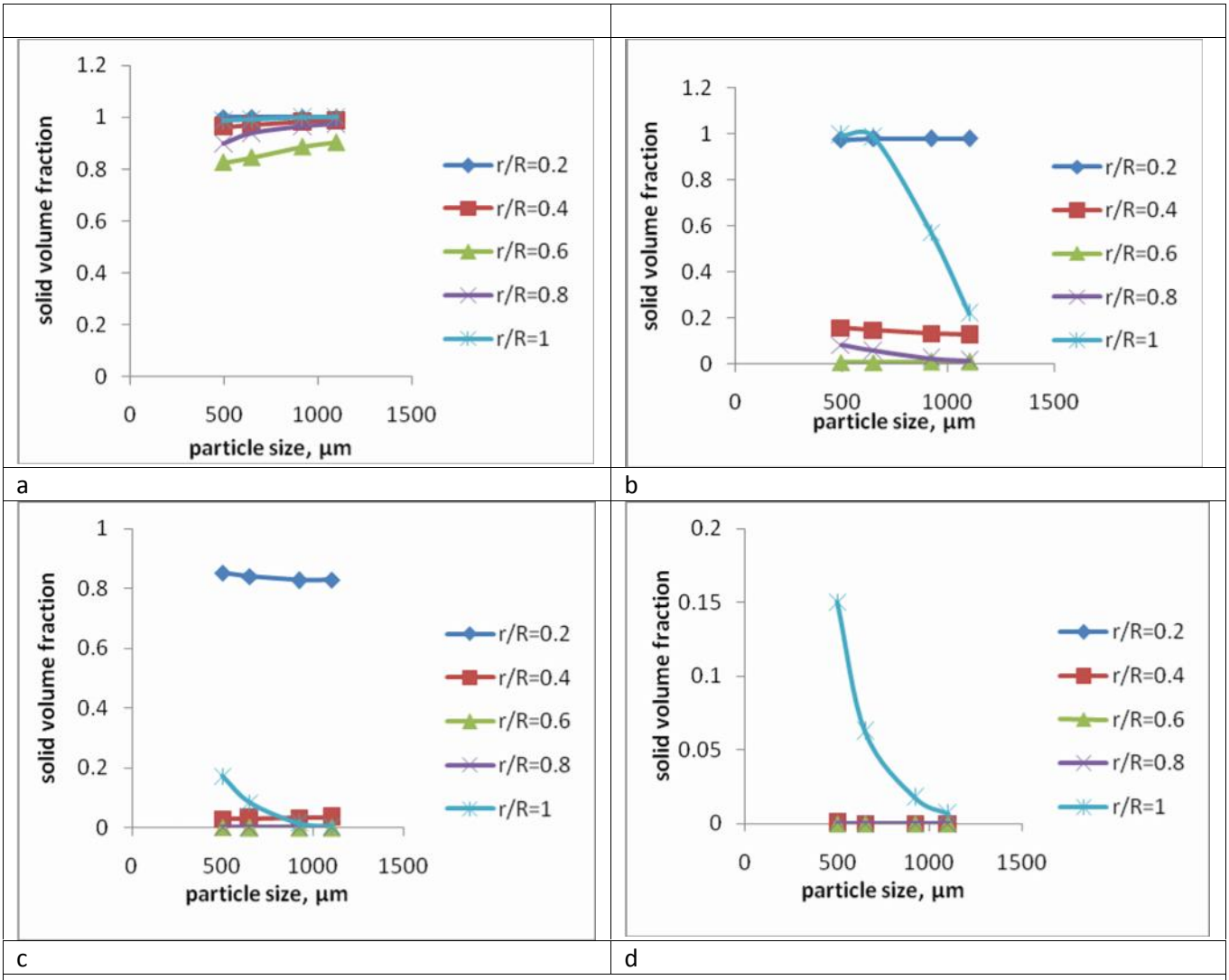

Fig .13. The variation of solid volume fraction with different particle sizes at various heights (a) z/H=0.1 (b) z/H=0.2 (c) z/H=0.3 (d) z/H=0.4

Figure 12 shows variation of solid volume fraction for various solids of size 500 µm at various heights. Figure 13 shows the variation of solid volume fraction for various size of same material at different heights. It is observed that the solid volume fraction decreases with increase in solid density and solid size at all heights for all radial positions and it is more significant at higher heights.

5. CONCLUSION

In this work, variation of solid volume fraction both in radial and axial direction in a stirred vessel driven by a Rushton turbine for different sizes and density were simulated by CFD using frozen rotor steady state approach. Radial Solid concentration profile is similar for different sizes except near the wall. The axial solid concentration profile is observed to be a similar pattern for different density particles and different sizes within this closer range. At a speed of 300 rpm non homogeneity was observed in both axial and radial direction and it was also found that solid volume fraction profile in the radial direction was similar for different sizes except near the wall as the range of variables(particle size and density) selected for the present study is of closer range. It was observed that the solid volume fraction decreased with the increase in solid density and solid size at all heights for all radial positions and it is more significant at higher heights.

NOMENCLATURE

C_D	drag coefficient
C_{TD}	momentum transfer coefficient for inter drag force
$C_{\varepsilon 1}$	k-ε turbulence model constant
$C_{\varepsilon 2}$	k-ε turbulence model constant
C_μ	k-ε turbulence model constant
k	turbulent kinetic energy per unit mass, m^2/s^2
$\vec{F}_i$	total interfacial force N/m^3
$\vec{F}_i^D$	interfacial force due to drag, N/m^3
$\vec{F}_i^T$	interfacial force due to turbulent dispersion, N/m^3
$\vec{F}_C$	centrifugal and coriolis forces, N/m^3
g	acceleration due to gravity, m/s^2
D	impeller diameter
d_p	particle diameter
c	bottom clearance, m
H	liquid height, m
N	impeller rotational speed, rpm
r	radial position, m
R	tank radius, m
T	tank diameter, m
w	blade width, m
z	axial position, m

Symbols

α	volume fraction
ε	turbulence dissipation rate, m^2/sec^2
μ	viscosity of liquid, Pa s
μ_{tl}	liquid phase kinematic eddy viscosity, m^2/sec
$\mu_{tl,p}$	particle induced turbulent viscosity, kg/m sec
$\mu_{tl,s}$	shear induced turbulent viscosity, kg/m sec
μ_{ts}	solid phase kinematic eddy viscosity, m^2/sec
ν	kinematic viscosity, m^2/sec
ρ	density, kg/m^3
σ_t	turbulent Prandtl number
σ_{tl}	turbulent Schmidt number
σ_k	turbulence model constant
σ_ε	k-ε turbulence model constant

REFERENCES

1. Ayazi Shamlou, P., Koutsakos, E., 1989. Solids suspension and distribution in liquids under turbulent agitation. Chemical Engineering Science 44 (3), 529–542.
2. Magelli, F., Fajner, D., Nocentini, M., Pasquali, G., 1990. Solid distribution in vessels stirred with multiple impellers. Chemical Engineering Science 45 (3), 615–625.
3. Barresi, A., Baldi, G., 1987. Solid dispersion in an agitated vessel: effect of particle shape and density. Chemical Engineering Science 42 (12), 2969–2972.

4. MacTaggart, R.S., Nasr-El-Din, H.A., Masliyah, J.H., 1993b. Sample withdrawal from a slurry mixing tank. Chemical Engineering Science 48 (5), 921–931.
5. Barresi, A.A., Kuzmanic, N., Baldi, G., 1994. Continuous sampling of slurry from a stirred vessel: analysis of the sampling efficiency and affecting parameters. Institution of Chemical Engineers Symposium Series 136, 17–24.
6. Nasr-El-Din, H.A., Mac Taggart, R.S., Masliyah, J.H., 1996. Local solid concentration measurement in a slurry mixing tank. Chemical Engineering Science 51 (8), 1209–1220.
7. Spidla, M., Sinevic, V., Jahoda, M., Machon, V., 2005. Solid particle distribution of moderately concentrated suspensions in a pilot plant stirred vessel. Chemical Engineering Journal 113, 73–82.
8. Considine, D.M., Considine, G.D., 1985. Process Instruments and Controls Handbook. McGraw-Hill, New York.
9. Mann, R., Stanley, S., Vlaev, D., Wabo, E., 2001. Augmented-reality visualization of fluid mixing in stirred chemical reactors using electrical resistance tomography. Journal of Electronic Imaging 10, 620–629.
10. Boyer, C., Duquenne, A.-M., Wild, G., 2002. Measuring techniques in gas-liquid and gas–liquid–solid reactors. Chemical Engineering Science 57 (16), 3185–3215.
11. Chaouki, J., Larachi, F., Dudukovic, M.P., 1997. Noninvasive Tomographic and Velocimetric Monitoring of Multiphase Flows. Elsevier Science, Amsterdam.
12. Esmaeili, B., Chaouki, J., Dubois, C., 2008. An evaluation of the solid hold-up distribution in a fluidized bed of nano particles using radioactive densitometry and fibre optics. Canadian Journal of Chemical Engineering 86 (3), 543–552.
13. Rasteiro, M.G., Figueiredo, M.M., Freire, C., 1994. Modeling slurry mixing tanks. Advanced Powder Technology 5, 1–14.
14. Sessiecq, P., Mier, P., Gruy, F., Cournil, M., 1999. Solid particles concentration profiles in an agitated vessel. Chemical Engineering Research and Design 77, 741–746.
15. Yamazaki, H., Tojo, K., Miyanami, K., 1986. Concentration profiles of solids suspended in a stirred tank. Powder Technology 48(3), 205–216.
16. Brucato, A., Magelli, F., Nocentini, M.G., Rizzuti, L., 1991. An application of the network of zones model to solid suspension in multiple impeller mixers. Chemical Engineering Research and Design 69, 43–52.
17. McKee, S.L., Williams, R.A., Boxman, A., 1995. Development of solid–liquid mixing models using tomographic techniques. The Chemical Engineering Journal 56, 101–107.
18. Divyamaan Wadnerkar., Ranjeet P.Utikar., Moses O.Tade.,Vishnu K.Pareek.,2012 CFD simulation of solid-liquid stirred tanks, Advanced powder Technology 23, 445-453.
19. Micale, G., Grisafi F., Rizzuti L., and Brucato A., 2004, CFD simulation of particle suspension height in stirred vessels, Chemical Engineering Research and Design 82, 1204-1213.
20. Zuoliang Sha., Seppo Palosaari, Pekka Oinas and Kohei Ogawa., 2001, CFD simulation of solid suspension in a stirred tank, Journal of Chemical Engineering of Japan, 34,621-626.
21. Rouzbeh Jafari., Phillippe A.Tanguy, Jamal Chaouki., 2012, Experimental investigation on solid dispersion, power consumption and scale-up in moderate to dense solid-liquid suspensions, Chemical Engineering Research and Design, 90, 201-212.
22. Nouri. J.M., Whitelaw J.H., 1992, Particle velocity characteristics of dilute to moderately dense suspension flows in stirred reactors, Int. J. Multiphase Flow, 18, 21-33.

*****